Research Article

Yao Ju*, Ievgen Konoplianchenko, Jiafei Pu, Qi Dong, and Zhengchuan Zhang

Structural characteristics and high-temperature friction properties of a solid metal surface with a laser-melted coating of high-entropy alloy

https://doi.org/10.1515/mgmc-2024-0004
received February 20, 2024; accepted April 15, 2024

Abstract: This article presents the results of a study on composite coatings based on high-entropy FeCoNiCrCuNb alloys with varying niobium content obtained through high-speed laser cladding. The primary objective of the research is to investigate the influence of composition on the structure, mechanical characteristics, and behaviour of the coatings. Microstructure analyses were performed using scanning electron microscopy and energy-dispersive spectroscopy analysis. The microhardness, shear strength, and coefficient of friction of the composite coatings were examined. It was demonstrated that the microstructure of the coatings is characterized by fine grains and the presence of columnar crystals. An increase in copper content leads to a transition to the face-centred cubic phase with elevated niobium content, influencing the mechanical characteristics. It was revealed that niobium-containing composite coatings exhibit improved mechanical properties and wear resistance. The incorporation of niobium synergistically affects the mechanical characteristics of the alloys. The obtained results hold practical applicability in the field of engineering, particularly where wear resistance and strength are of paramount importance.

Keywords: high-entropy alloys, laser cladding, mechanical properties, microstructure, niobium, microhardness, shear strength, friction, wear.

*** Corresponding author: Yao Ju,** School of Transportation, Xinxiang Vocational and Technical College, Xinxiang, China; Technical Services Department, Sumy National Agrarian University, Sumy, Ukraine, e-mail: juyao831214@xxvtc.edu.cn
Ievgen Konoplianchenko, Jiafei Pu, Qi Dong, Zhengchuan Zhang: Technical Services Department, Sumy National Agrarian University, Sumy, Ukraine

1 Introduction

In recent years, an increasing amount of attention from researchers has been directed towards multi-component high-entropy alloys (HEAs) [1,2]. Due to the synergy of high entropy, lattice distortion, sluggish diffusion, and the cocktail effect, HEAs have garnered interest for their exceptional physical and mechanical properties [3]. Consequently, both HEAs and their affiliated composites exhibit significant potential for engineering applications [4,5].

Unlike conventional alloys, which typically consist of a single base element, such as aluminium alloys, titanium alloys, or iron alloys [6], HEAs embody an innovative approach to alloy design [7]. HEAs, also referred to as multi-component alloys, are broadly defined as solid solution alloys comprising more than five primary elements with relatively equiatomic percentage composition (at%). This approach involves the incorporation of a substantial number of elements or components (usually five or more) with concentrations ranging from 5 to 35 at%. They have emerged as promising candidates with elevated potential for application in tools, dies, and structural components [5,8]. Numerous investigations have demonstrated the enhancement of microhardness and wear resistance through selective adjustment of multiple constituents within HEAs [9]. HEAs also exhibit solid solution strengthening and antioxidant protection properties at elevated temperatures [10]. HEAs have become promising candidates capable of satisfying the demands of intricate, extreme, and highly sensitive service environments, particularly within the nuclear, turbine, and aerospace sectors [11].

The investigation of stability or metastability of high-entropy phases commenced shortly after the discovery of HEAs and remains a subject of discourse to this day. Precursors to these alloys can be identified in bulk amorphous alloys, also recognized as metallic glasses. Upon solidification from the molten state, they form a singular phase [12]. Upon heating, this phase undergoes devitrification, transitioning into a crystalline state and occasionally segregating into multiple phases [13].

In contrast to metallic glasses, atoms in HEAs assume simpler crystalline structures, namely, face-centred cubic (FCC), hexagonal close-packed, and body-centred cubic (BCC) lattices upon crystallization from the molten state. Various types of atoms are randomly situated at lattice sites, resulting in HEAs being unordered substitutional solid solutions. The disordered arrangement of all atoms at lattice nodes leads to heightened configurational entropy in this phase, thereby accounting for the nomenclature attributed to this class of materials [14,15].

Laser cladding technology represents a cost-effective approach to applying specialized coatings to conventional metallic substrates. Consequently, the laser cladding technique is gaining increasing traction for the production of HEAs [16–18].

Qiu et al. [19] performed coating of an HEA $Al_2CrFeCo_x$-CuNiTi onto Q235 steel. They extensively discussed the influence of Co content on the microstructure of the coating and its corrosion resistance. Remarkably, the presence of Co accelerates the formation of a passive film on the surface of the plated layer under the influence of H_2SO_4 and HCl solutions, leading to enhanced corrosion resistance [19]. Xulong and Qibin [20] discovered that the incorporation of WC particles into an HEA SiFeCoCrTi coating increases both microhardness and wear resistance. The presence of WC particles had a noticeable impact on the shell layer, inducing a shift in the lattice structure from FCC to BCC, alongside the formation of various intermetallic compounds [20]. Huang et al. [21] employed laser cladding to generate a layer of HEA AlCrNiSiTi on the surface of Ti–6Al–4V alloy (Ti64). This study revealed that the introduction of the (Ti, Cr)(5)Si-3 phase enhances the wear resistance of the coating [21]. Sha et al. [22] subjected a layer of HEA AlCoCrFeNiTi0.5 to annealing at 900°C for 5 h, resulting in the emergence of new phases within the coating (namely, $Al_{80}Cr_{13}Co_7$, Co_3Ti, and AlFe). This led to an overall increase in the average microhardness of the coating, subsequently reducing wear losses and crack width during grinding [22]. Wang et al. [23] investigated the influence of diamond additives on the properties of an HEA composition FeCoCrNi-Mo. The investigation emphasizes the intricate interplay between laser cladding parameters and the resultant microstructure and properties of composite coatings. It is noted that as laser power increases, micro-pores, cracks, and diamond graphitization become more pronounced, resulting in decreased hardness and deterioration resistance. Similarly, excessively low scanning speeds enhance energy absorption by the powder and intensify diamond graphitization, while excessively high scanning speeds lead to unmelted HEA powders and suboptimal bonding between the HEA matrix and diamond [23].

The efficacy of incorporating Nb as an element for enhancing hardness and deterioration resistance in high-entropy systems is well justified. The study by Qin et al. [24] underscored the favourable influence of Nb inclusion in various HEA systems. In the CoCrCuFeNiNb HEA system, Nb contributed to a transition from the FCC phase to the Laves phase, thereby enhancing the compressive yield strength [24]. Feng and colleagues [25] demonstrated that introducing Nb into dense high-entropy (Hf, Zr, Ti, Ta, Nb) ceramics led to the formation of second phases rich in Nb, effectively impeding grain growth and elevating hardness. In the investigation conducted by Luo et al. [26], a composite consisting of WC + Al_xCrFeCoNiCu (with $0 \le x \le 1.5$) was meticulously prepared. This involved the blending of WC with powders of Al, Cr, Fe, Co, Ni, and Cu, followed by plasma sintering. The gradual diffusion process resulted in the dispersion of WC particles within the solid solution phase of the HEA. Notably, the WC + $Al_{0.5}$CrFeCoNiCu composite exhibited remarkable mechanical properties, particularly displaying a high hardness of 2071 HV30 and an impressive fracture toughness of 10.3 MPa.

To mitigate defects arising from significant mismatches in thermo-physical properties between the coating and substrate, ensuring compatibility and resemblance between the HEA powder and the substrate is imperative. Hence, the selection of HEA constituents for this experiment encompassed Fe, Co, Ni, Cr, Cu, and Nb. Each element was strategically chosen for its distinct contributions. The objective of this study is to investigate the microstructure, mechanical, and tribological properties of composite coatings based on FeCoNiCrCu-Nb HEAs and their influence on enhancing wear resistance and mechanical strength under varying load and friction conditions. To achieve the established research objective, the following tasks were formulated:

(1) Perform an analysis of the microstructure of composite coatings based on FeCoCrNi-Mo HEAs with varying niobium contents.
(2) Evaluate the microhardness and shear strength of coatings at different copper and niobium contents and compare them with the mechanical characteristics of the substrate.
(3) Investigate the tribological properties of composite coatings, encompassing friction coefficient and wear resistance, under diverse load and friction conditions.

2 Materials and methods

2.1 Characterization of the investigated objects

As the substrate material for this investigation, an iron–aluminium alloy was chosen due to its excellent balance between strength and corrosion resistance. The chemical composition of the iron–aluminium alloy is provided in Table 1.

The experimental procedures employed samples with dimensions of 70 mm × 40 mm × 10 mm. To mitigate the potential influence of an oxide film on the substrate surface, which could impact coating adhesion, a preparatory step involving abrasive paper with a grit size of 1,000 was utilized to polish the substrate surface before laser cladding. Subsequently, the substrate was immersed, initially in a saturated solution of potassium hydroxide, followed by a diluted solution of nitric acid, ensuring complete removal of the oxide film.

To achieve effective powder dispersion and controlled delivery, spherical or near-spherical metallic powders of Fe, Co, Ni, Cr, Cu, and Nb ($Fe_{0.7}CoNiCrCuNb_x$) were meticulously selected with special consideration, exhibiting a high level of purity (99.99%). These metallic powders were procured from Changsha Tianjiu Company. The granulometric distribution of these powders ranges from 100 to 200 mesh. The precise proportions of powders and their corresponding alloy designations are listed in Table 2.

To achieve uniform blending, the mixed powder was ball-milled in a controlled environment for 3 h. After this, the milled powder was meticulously dried for 3 h under vacuum conditions. The powder was then hermetically sealed and stored within a controlled atmosphere.

Table 1: Chemical composition of the alloy

Component	Fe	Al	Mn	C
Content (wt%)	89.5	5	5	0.5

2.2 Coating application

The deposition process was performed utilizing a JK2003SM Nd: YAG laser machine. Optimized process parameters were employed, including a spot diameter of 1.2 mm, a laser power of 1,850 W, a powder feed rate of 5.6 g·min^{-1}, a scanning speed of 120 mm·min^{-1}, a fill factor of 70%, a pulse frequency of 50 Hz, an overlap rate of 30%, and a carrier gas flow rate of 5 L·min^{-1} [27].

2.3 Microstructure and composition analysis

Microstructure investigation and chemical composition analysis were conducted using a scanning electron microscope (SEM, FEI, Quanta 250 FEG, Vlastimila Pecha, Czech Republic), equipped with an energy-dispersive spectrometer (EDS).

2.4 Material assessment

The alloy hardness was determined using a Vickers hardness tester (BUEHLER 5104, Buehler, Lake Bluff, USA) under a load of 250 g for 20 s, with the mean value computed from three measurements.

The wear resistance of the alloy was assessed using a high-speed reciprocating motion friction test instrument, HRS-2M (HRS-2M, Zhongke Kaihua, Lanzhou, China). The test conditions were the following: a friction time of 45 min, a load of 70 N, a frequency of 20 Hz, and a stroke length of 7 mm. The wear test was conducted under standard atmospheric pressure and room temperature. A GCr15 steel ring with a hardness of 63 HRC, a diameter of 55 mm, and a thickness of 12 mm was utilized as the wear track. Wear samples were sized at 8 mm × 16 mm × 12 mm. Before wear testing, the coating surface underwent meticulous grinding, polishing, acetone cleaning, and drying procedures. Throughout the entire wear test, the

Table 2: Chemical composition of $Fe_{0.7}CoNiCrCuNb_x$

Abbreviation	Alloy	Component content (%)					
		Fe	Co	Ni	Cr	Cu	Nb
Nb_0	$Fe_{0.7}CoNiCrCu$	14.9	21.3	21.3	21.3	21.3	0.0
$Nb_{0.25}$	$Fe_{0.7}CoNiCrCuNb_{0.25}$	14.1	20.2	20.2	20.2	20.2	5.1
$Nb_{0.5}$	$Fe_{0.7}CoNiCrCuNb_{0.5}$	13.5	19.2	19.2	19.2	19.2	9.6
$Nb_{0.75}$	$Fe_{0.7}CoNiCrCuNb_{0.75}$	12.8	18.3	18.3	18.3	18.3	13.8
Nb_1	$Fe_{0.7}CoNiCrCuNb$	12.3	17.5	17.5	17.5	17.5	17.5

frictional moment was measured at 5-min intervals to calculate the coefficient of friction of the sample using the following equation:

$$\mu = \frac{M}{Fr}$$

where μ is the coefficient of friction, M is the frictional moment, F is the applied load, and r is the radius of the compensation ring.

To investigate the influence of varying niobium (Nb) content on the coating adhesion quality, a cylindrical sleeve was fabricated from quenched high-strength steel with dimensions of 50 mm × 100 mm. The Fe0.7CoNiCrCuNbx coating and relief plate were applied to the cylindrical surface of a rod made of iron–aluminium alloy with a diameter of 50 mm using laser cladding and turning processes, respectively. The raised plate had a width of 0.8 mm and a height of 2 mm. The shear force was evaluated using a universal testing machine DNS100, and the quality of the bond, reflecting shear stress (or shear strength, σ), was calculated using the equation:

$$\sigma = \frac{F_{\mathrm{M}}}{\pi D s}$$

where F_{M} is the maximum shear load, D is the diameter of the specimen, and s is the width of the coating.

3 Results and discussion

SEM images illustrating cross-sectional views and microstructures of the coatings are shown in Figure 1. The specimens were cut perpendicular to both the direction of laser cladding and the substrate surface. No significant differences in microstructures are observed. On the surface of the coating, grains appear fine, except for the presence of columnar crystals. The angle formed between the columnar crystals and the laser-clad direction is extremely small. Consequently, the cross-sectional area occupied by these columnar crystals on the surface is also limited. The microstructure of the surface is characterized by fine grains. The results of the EDS analysis for each region in Figure 1 are summarized in Table 3. Light zones (LZ) and dark zones (DZ) appear at grain boundaries. EDS data reveal that the Nb content in LZ significantly exceeds the nominal composition (Table 3). In the Nb_0 alloy, a high-impact resistant FCC phase is present, inhibiting the release of lattice distortion energy near the grain boundary through the cross-slip of screw and edge dislocations during cooling. With an increase in Nb content to 0.25 LP, a chain-like configuration is adopted along the grain boundary (Figure 1b).

Unlike the $Nb_{0.25}$ alloy, the $Nb_{0.5}$, $Nb_{0.75}$, and $Nb_{1.0}$ alloys exhibit a reticular structure. EDS analysis confirms the segregation of Nb within the zones (Table 3). By

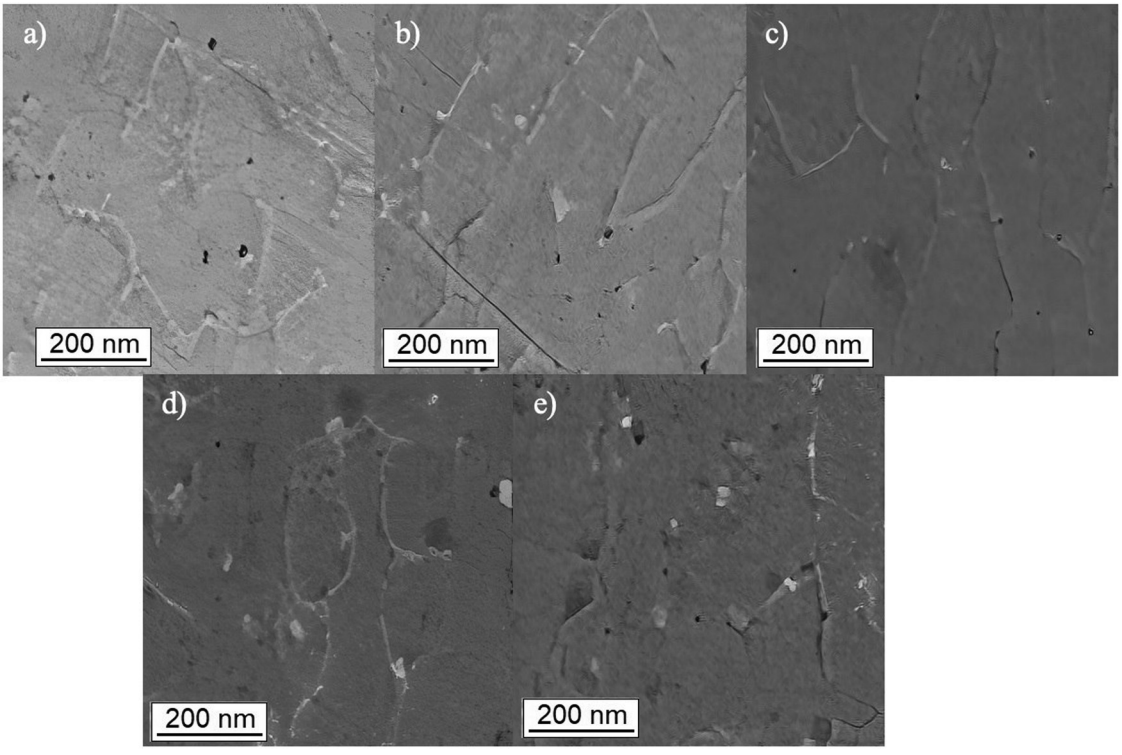

Figure 1: SEM images illustrating cross-sectional views and microstructures of the alloys: (a) Nb_0, (b) $Nb_{0.25}$, (c) $Nb_{0.5}$, (d) $Nb_{0.75}$, and (e) Nb_1.

Table 3: Analysis of the energy spectrum

Nb	Zone	Fe	Co	Ni	Cr	Cu	Nb
0.25	Nominal	14.14	20.20	20.20	20.20	20.20	5.05
	LZ	15.38	15.12	16.64	12.56	15.06	24.42
	DZ	13.04	20.18	15.90	24.17	21.79	5.07
0.5	Nominal	13.46	19.23	19.23	19.23	19.23	9.62
	LZ	16.63	13.44	14.67	12.70	14.76	27.38
	DZ	16.26	20.23	15.90	20.10	21.36	5.79
0.75	Nominal	12.84	18.35	18.35	18.35	18.35	13.76
	LZ	16.26	15.00	17.17	11.22	14.12	25.77
	DZ	14.65	19.34	19.74	18.97	19.62	7.46
1	Nominal	12.28	17.54	17.54	17.54	17.54	17.54
	LZ	16.25	12.64	20.90	9.71	10.11	29.84
	DZ	14.12	18.18	17.23	17.85	18.78	13.59

correlating these observations with the data, it can be inferred that the increase in copper content leads to a transition from a point-like distribution to a continuous distribution of the Nb-rich FCC phase in the $Fe_{0.7}CoNiCrCuNb_x$ HEA with laser cladding. However, in the Nb1.0 alloy, a crack is observed along the grain boundary (Figure 1e). Examining the crack characteristics and EDS results, it can be deduced that the following factors contribute to crack formation: a significant difference in melting temperatures between the substrate and the tested powder results in a substantial temperature gradient within the molten pool during the LP process.

In Figure 2, the average microhardness values of $Fe_{0.7}CoNiCrCuNb_x$ (x = 0, 0.25, 0.5, 0.75, 1.0) HEA coatings along with the substrates are presented. The Nb1.0 alloy lacks the BCC phase. This crystalline structure has fewer available slip planes, leading to reduced deformation under load and, consequently, the lowest observed hardness among the Nb_0 alloys. As the Nb content increases, the BCC phase in the $A_{l0.8}CrFeCoNiCu_x$ HEA also increases. Coatings with niobium content (especially beyond 0.25) exhibit improved mechanical properties, suggesting enhanced resistance to wear and deformation. The data indicate that the influence of niobium on hardness is not merely additive; it can exert a synergistic effect with other alloying elements, contributing to the observed enhancements. The FCC structure possesses more slip directions in the slip plane compared to the BCC structure. This structural distinction facilitates plastic deformation under load, resulting in a gradual reduction in the hardness of $Fe_{0.7}CoNiCrCuNb_x$ HEA. Overall, the HEA coating $Fe_{0.7}CoNiCrCuNb_x$ demonstrates significantly higher hardness (approximately 6–7 times) than the substrate.

The substrate exhibits a shear strength of 265.7 MPa, as indicated in Figure 3. Shear data for $Nb_{0.25}$, $Nb_{0.5}$, $Nb_{0.75}$, and $Nb_{1.0}$ reveal a zone of plastic deformation indicative of plastic failure. The corresponding shear strength values for these compositions are 162.0, 221.5, 197.6, and 179.2 MPa, representing 61.0%, 83.4%, 74.4%, and 67.4% of the substrate's strength, respectively. The low shear strength of Nb_0 hinders the establishment of a reliable coating-substrate bond. A shear strength of 102.4 MPa corresponds to 38.5% of the substrate's strength. Consequently, we will not further investigate the properties of the $Fe_{0.7}CoNiCrCu$ alloy in the subsequent analysis.

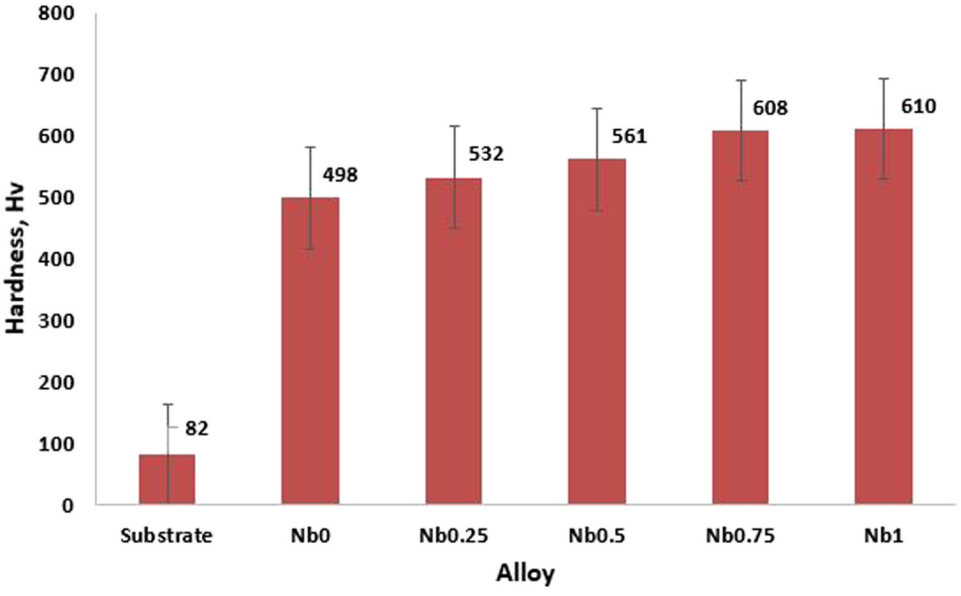

Figure 2: Hardness of the alloys.

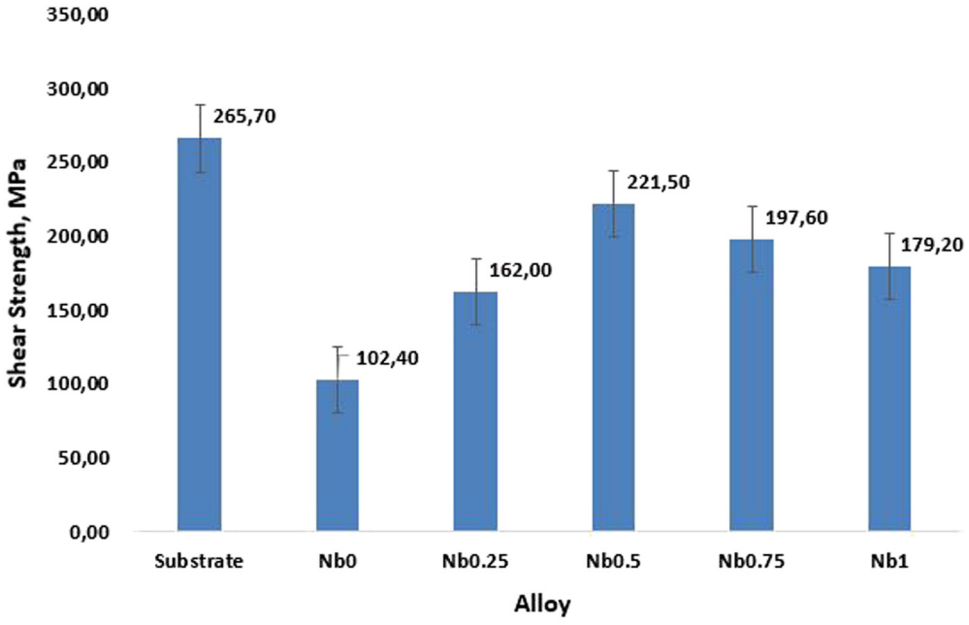

Figure 3: The shear strength of the alloys.

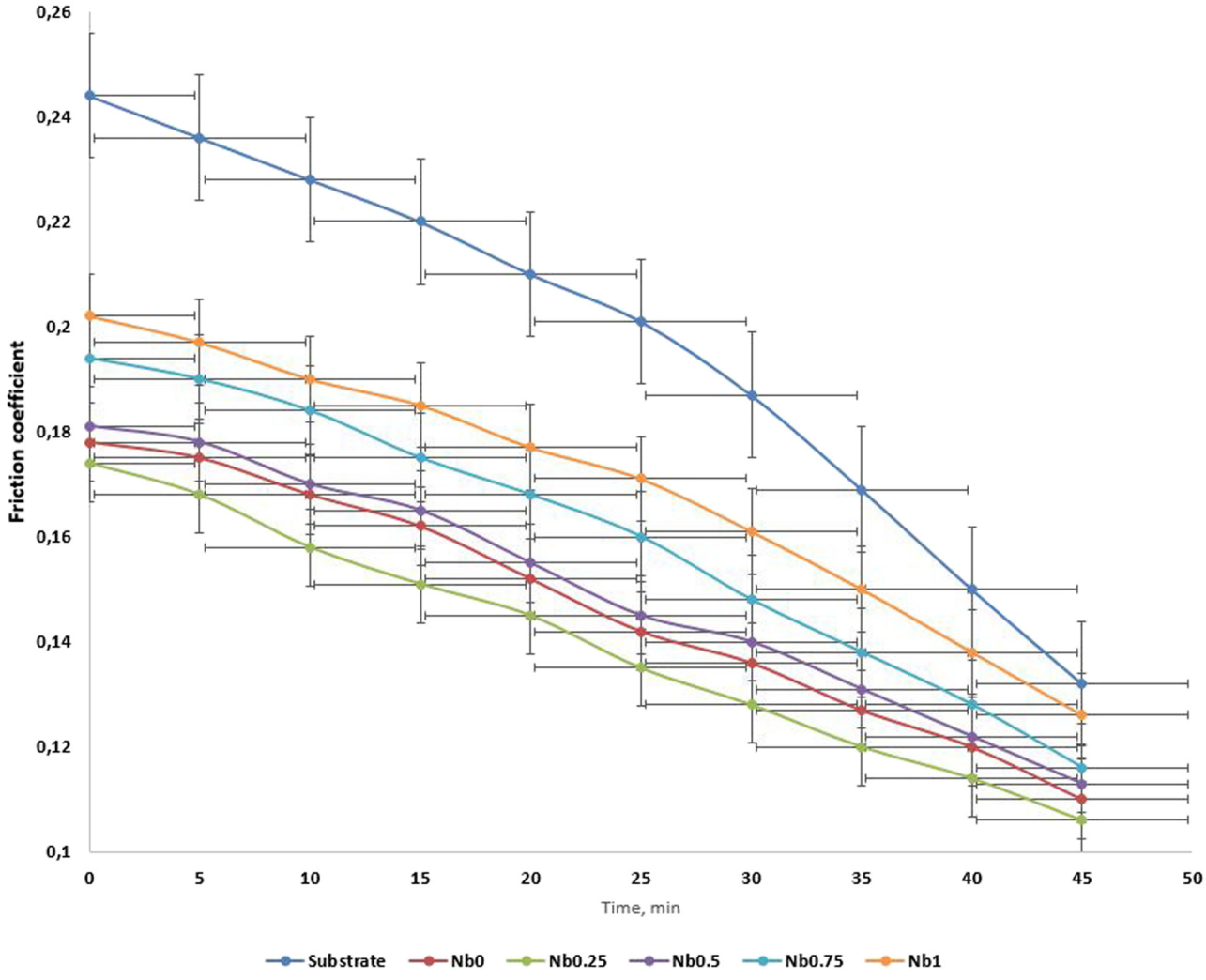

Figure 4: Friction coefficient of the alloys.

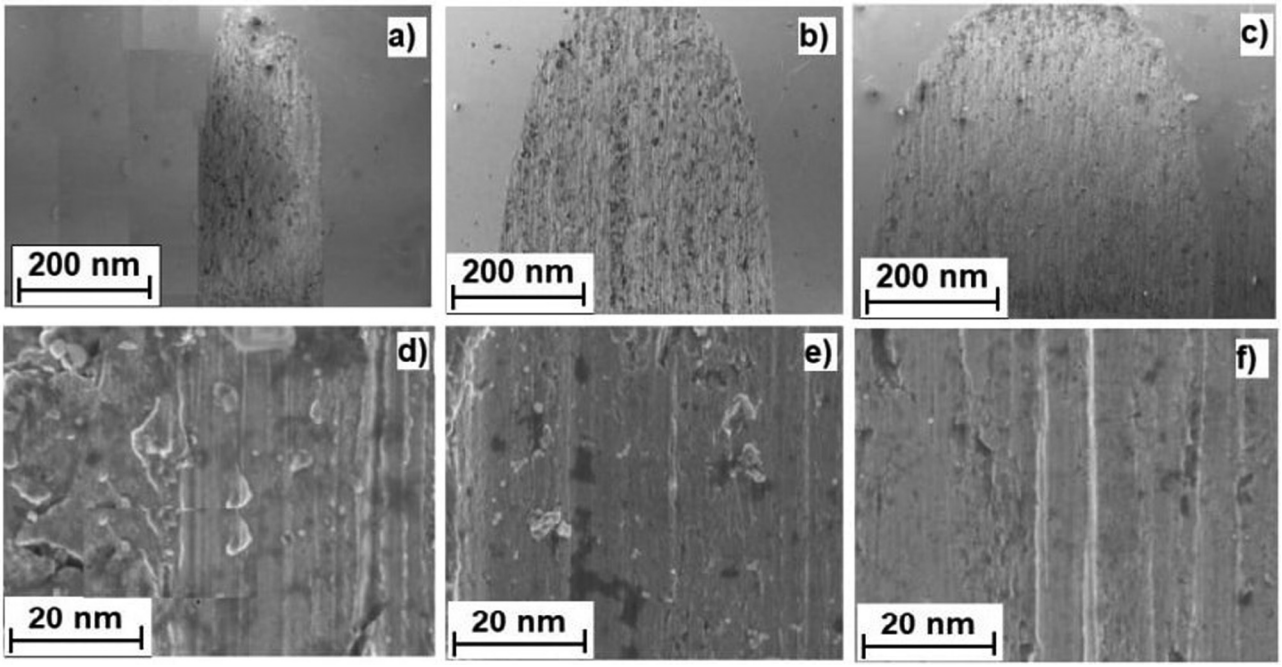

Figure 5: Secondary electron SEM images of wear tracks on the Fe0.7CoNiCrCuNb sample: (a) and (d) after 5 min, (b) and (e) after 25 min, and (c) and (f) after 45 min.

Figure 4 depicts the friction coefficient curves of both the substrate and the $Fe_{0.7}CoNiCrCuNb_x$ HEA coatings (x = 0.25, 0.5, 0.75, 1). It can be observed that the friction coefficient of each specimen tends to decrease with increasing wear time. The friction coefficient of the $Fe_{0.7}CoNiCrCuNb_x$ coatings was notably lower than that of the substrate. As the Cu content increases, the friction coefficient of $Fe_{0.7}CoNiCrCuNb_x$ tends to increase.

Figure 5 exhibits SEM studies of the wear tracks seen in the Fe0.7CoNiCrCuNb sample. Figure 5a–c illustrates the worn surface of the sample, clearly indicating the presence of abrasive wear. The SEM images of the wear tracks show the presence of abrasion and debris on the sample surface during a 5-min wear interval. With the prolonged period of the test, the debris was progressively eliminated.

As previously mentioned, significant thermal stresses arise within the coating. A similar phenomenon was observed in the AlCrFeCoNi HEA coating deposited by laser spraying onto pure aluminium by Soni et al. [28] and Zhang et al. [29]. Notably, the Fe content in the samples typically exceeds the nominal composition (Table 3), indicating Fe migration during LP. The composition of the dark grey phase closely resembled the theoretical composition of the FeCoCrNi-Mo HEA matrix, reinforced with intermediate solid solution strengthening through the inclusion of C elements. The light grey phase exhibited relatively elevated Nb content and reduced Cr content. A similar role was played by molybdenum in facilitating the FCC to σ-phase transition in the FeCoCrNi system [30,31]. Composite coatings of FeCoCrNi-Mo with diamonds were successfully obtained through high-speed laser cladding. The incorporation of diamonds into the composite coating improved wear resistance, albeit leading to an increased occurrence of microcracks. It is noteworthy that an optimal combination of microstructural characteristics and wear resistance was achieved with a volume fraction of 15% diamonds. In our study, the hardness of the initial alloy significantly exceeded that of the substrate, with niobium also employed as an additional material, contributing to the enhanced hardness of such a coating [23].

In wear testing, the material undergoes various stages of wear: the initial running-in stage, the stable wear stage, and the intensive wear stage [32,33] causing a gradual decrease in the friction coefficient. The friction coefficient of the $Fe_{0.7}CoNiCrCuNb_x$ alloy is proportional to the Nb content, as the addition of Nb increases the proportion of the FCC phase.

4 Conclusions

Using high-speed laser cladding, it was successfully possible to synthesize HEA coatings of $Fe_{0.7}CoNiCrCuNb_x$ (x = 0, 0.25, 0.5, 0.75, 1) and determine the optimal process parameters yielding superior mechanical properties. Microstructural

analysis revealed a significant influence of niobium content on the structure and properties of the coatings. Coatings with elevated niobium content exhibited enhanced mechanical characteristics: at a niobium content of 0.25%, a reduction in shear strength to 61.0% of the substrate's strength was observed, while coatings with niobium content above 0.25% demonstrated considerable growth in shear strengths to 83.4%, 74.4%, and 67.4% of the substrate's strength, respectively. This effect is elucidated by the synergy between niobium and other alloying elements within the HEA, leading to observed enhancements in coating hardness and structure.

Hence, this study makes a substantial contribution to the advancement of understanding and utilization of HEA coatings with enhanced mechanical properties, holding potential for application across diverse engineering and industrial domains.

Funding information: Authors state no funding involved.

Author contribution: All authors have accepted responsibility for the entire content of this manuscript and consented to its submission to the journal, reviewed all the results and approved the final version of the manuscript. Yao Ju, Ievgen Konoplianchenko and Jiafei Pu designed the experiments and Qi Dong and Zhengchuan Zhang carried them out. Yao Ju prepared the manuscript with contributions from all co-authors.

Conflict of interest: Authors state no conflict of interest.

Data availability statement: The datasets generated during and/or analyzed during the current study are available from the corresponding author on reasonable request.

References

[1] İroç LK. Development and production of Ductile TiZrNbHfTa refractory high entropy alloy system for extreme environments. Master's thesis. Middle East Technical University, Ankara, Turkey, 2022.

[2] Grilli ML, Valerini D, Slobozeanu AE, Postolnyi BO, Balos S, Rizzo A, et al. Critical raw materials saving by protective coatings under extreme conditions: A review of last trends in alloys and coatings for aerospace engine applications. Materials. 2021;14(7):1656. doi: 10.3390/ma14071656.

[3] Hua X-J, Hu P, Xing H-R, Han J-Y, Ge S-W, Li S-L, et al. Development and property tuning of refractory high-entropy alloys: A review. Acta Metall Sin (Eng Lett). 2022;35(8):1231–65. doi: 10.1007/s40195-022-01382-x.

[4] Chang X, Zeng M, Liu K, Fu L. Phase engineering of high-entropy alloys. Adv Mater. 2020;32(14):1907226. doi: 10.1002/adma.201907226.

[5] Zhai W, Bai L, Zhou R, Fan X, Kang G, Liu Y, et al. Recent progress on wear-resistant materials: designs, properties, and applications. Adv Sci. 2021;8(11):2003739. doi: 10.1002/advs.202003739.

[6] Yurtkuran H. An evaluation on machinability characteristics of titanium and nickel-based superalloys used in the aerospace industry. İmalat Teknol Uygulamaları. 2021;2(2):10–29. doi: 10.52795/mateca.940261.

[7] Chi Y, Gu G, Yu H, Chen C. Laser surface alloying on aluminum and its alloys: a review. Opt Laser Eng. 2018;100:23–37. doi: 10.1016/j.optlaseng.2017.07.006.

[8] Gorsse S, Couzinié JP, Miracle DB. From high-entropy alloys to complex concentrated alloys. Comp Rend Phys. 2018;19(8):721–36. doi: 10.1016/j.crhy.2018.09.004.

[9] Lindner T, Löbel M, Sattler B, Lampke T. Surface hardening of FCC phase high-entropy alloy system by powder-pack boriding. Surf Coat Technol. 2019;371:89–94. doi: 10.1016/j.surfcoat.2018.10.017.

[10] Huang L, Cao Y, Zhang J, Dong AP, Tu J, Chai LJ, et al. Effect of heat treatment on the microstructure evolution and mechanical behaviour of a selective laser melted Inconel 718 alloy. J Alloy Comput. 2021;865:158613. doi: 10.1016/j.jallcom.2021.158613.

[11] Arshad M, Amer M, Hayat Q, Janik V, Zhang X, Moradi M, et al. High-entropy coatings (HEC) for High-temperature applications: materials. Proc Prop Coat. 2022;12(5):691. doi: 10.3390/coatings12050691.

[12] Edalati K, Akiba E, Botta WJ, Estrin Y, Floriano R, Fruchart D, et al. Impact of severe plastic deformation on kinetics and thermodynamics of hydrogen storage in magnesium and its alloys. J Mat Sci Technol. 2022;146:221–39. doi: 10.1016/j.jmst.2022.10.068.

[13] Hajas BI. Thermal stability and oxidation resistance of high-entropy sublattice nitrides. PhD dissertation. Storrs: Institute of Materials Science; 2021.

[14] Ter-Isahakyan A, Rau JS, Balk TJ. High entropy alloys with hexagonal close-packed structure derived from thin film combinatorial approach. J Alloy Compd. 2022;893:162293. doi: 10.1016/j.jallcom.2021.162293.

[15] Xie Z, Jian WR, Xu S, Beyerlein IJ, Zhang X, Yao X, et al. Phase transition in medium entropy alloy CoCrNi under Quasi-isentropic compression. Intern J Plast. 2022;157:103389. doi: 10.1016/j.ijplas.2022.103389.

[16] Behera A. High entropy materials. Advanced materials: an introduction to modern materials science. Cham: Springer; 2022. p. 291–320, doi: 10.1007/978-3-030-80359-9_9.

[17] Chen A, Zhuo L. Latest progress on refractory high entropy alloys: composition, fabrication, post processing, performance, simulation and prospect. Intern J Refract Met Hard Mater. 2022;110:105993. doi: 10.1016/j.ijrmhm.2022.105993.

[18] Saurabh A, Verma PC, Kumar A. Laser cladding: an innovative surface engineering technique for automotive brake discs. Las Eng. 2023;55(1/2):39–64.

[19] Qiu XW, Wu MJ, Liu CG, Zhang YP, Huang CX. Corrosion performance of Al2CrFeCoxCuNiTi high-entropy alloy coatings in acid liquids. J Alloy Compd. 2017;708:353–7. doi: 10.1016/j.jallcom.2017.03.054.

[20] Xulong A, Qibin L. Effect of WC particles on microstructure and properties of high entropy alloy SiFeCoCrTi coating synthesized by laser cladding. Rare Met Mat Eng. 2016;45(9):2424–8.

[21] Huang A, Tang YZ, Zhang YZ, Dong AP, Tu J, Chai LJ, et al. Microstructure and dry sliding wear behavior of laser clad AlCrNiSiTi multi-principal element alloy coatings. Rare Met. 2017;36(7):562–8. doi: 10.1007/s12598-017-0912-y.

[22] Sha M, Zhang L, Zhang J, Li N, Li T, Wang N. Effects of annealing on the microstructure and wear resistance of AlCoCrFeNiTi0.5 high-entropy alloy coating prepared by laser cladding. Rare Met Mat Eng. 2017;46(5):1237–40. doi: 10.1016/S1875-5372(17)30143-1.

[23] Wang H, Zhang W, Peng Y, Zhang M, Liu S, Liu Y. Microstructures and wear resistance of FeCoCrNi-Mo high entropy alloy/diamond composite. Coat High-Speed Laser Cladding. 2020;10(3):300. doi: 10.3390/coatings10030300.

[24] Qin G, Wang S, Chen R, Gong X, Wang L, Su Y, et al. Microstructures and mechanical properties of Nb-alloyed CoCrCuFeNi High-entropy alloys. J Mater Sci Technol. 2018;34(2):365–9. doi: 10.1016/j.jmst.2017.11.007.

[25] Feng L, Fahrenholtz WG, Hilmas GE, Monteverde F. Effect of Nb content on the phase composition, densification, microstructure, and mechanical properties of high-entropy boride ceramics. J Eur Ceram Soc. 2021;41(1):92–100. doi: 10.1016/j.jeurceramsoc.2020.08.058.

[26] Luo W, Liu Y, Shen J. Effects of binders on the microstructures and mechanical properties of ultrafine WC-10% AlxCoCrCuFeNi composites by spark plasma sintering. J Alloy Compd. 2019;791:540–9. doi: 10.1016/j.jallcom.2019.03.328.

[27] Zhang R, Gu X, Gong H, Gu X, Zhao X. Effect of Nb content on microstructure and properties of FeCoNi2CrMnV0.5NbX high-entropy alloy coatings by laser cladding. J Mat Res Technol. 2022;21:3357–70. doi: 10.1016/j.jmrt.2022.10.144.

[28] Soni VK, Sanyal S, Sinha SK. Influence of tungsten on microstructure evolution and mechanical properties of selected novel FeCoCrMnWX high entropy alloys. Intermetallics. 2021;132:107161. doi: 10.1016/j.intermet.2021.107161.

[29] Zhang M, Zhou X, Yu X, Li J. Synthesis and characterization of refractory TiZrNbWMo high-entropy alloy coating by laser cladding. Surf Coat Technol. 2017;311:321–29. doi: 10.1016/j.surfcoat.2017.01.012.

[30] Beketaeva AO, Naimanova AZ, Shakhan N, Zadauly A. Simulation of the shock wave boundary layer interaction in flat channel with jet injection. ZAMM-J Appl Math Mech. 2023;103(8):e202200375. doi: 10.1002/zamm.202200375.

[31] Moradi ST, Nikolaev NI. Chudinova IV. geomechanical analysis of wellbore stability in high-pressure, high-temperature formations. 79th EAGE Conference and Exhibition 2017, Vol. 2017, No. 1. Utrecht: European Association of Geoscientists & Engineers; 2017. p. 1–3. doi: 10.3997/2214-4609.201701463.

[32] Liu WH, Lu ZP, He JY, Luan JH, Wang ZJ, Liu B, et al. Ductile CoCrFeNiMoX high entropy alloys strengthened by hard intermetallic phases. Acta Mater. 2016;116:332–42. doi: 10.1016/j.actamat.2016.06.063.

[33] Zhou Y, Chen Z, Zhang T, Zhang S, Xing X, Yang Q, et al. Metastable hybridized structure transformation in amorphous carbon films during Friction – a study combining experiments and MD simulation. Friction. 2023;11:1708–23. doi: 10.1007/s40544-022-0690-x.